The Breakdown of Strength Size Scaling in Metallic Glass

S. Wang[1], Y.F. Ye[1], Q. Wang[2], S.Q. Shi[3], and Y. Yang[1,*]

[1]Centre for Advanced Structural Materials, Department of Mechanical and Biomedical Engineering, City University of Hong Kong, Kowloon Tong, Kowloon, Hong Kong SAR, China

[2]Laboratory for Microstructures, Institute of Materials Science, Shanghai University, Shanghai, China

[3]Department of Mechanical Engineering, the Hong Kong Polytechnic University, Hung Hom, Kowloon, Hong Kong SAR, China

It was previously reported that the strength of metallic glasses (MGs) would scale inversely with the size of a sample or a deformation field, commonly known as "smaller-being-stronger". However, based on the extensive spherical nanoindentation experiments conducted across a variety of MGs, we demonstrates that such strength-size scaling breaks down at a critical indenter tip radius, which is caused by the transition of the yielding mechanism from bulk- to surface-controlled shear band initiation. Our experimental findings not only shed quantitative insights into nano-scale incipient plasticity in MGs but also explain the unusual strength scattering observed in the nano-compression of MGs.

It is well known that the strength of crystalline metals usually increases as their size decreases[1]. This phenomenon of strength size effect could be generally ascribed to the interplay between external sizes, such that those associated with sample dimensions or deformation field, and internal sizes, such as grain size and dislocation spacing[2-7]. To

* Corresponding Author. Email: (YY) yonyang@cityu.edu.hk

quantify the strength size effect in crystalline metals, different scaling relations were established over the past decades, such as $\sigma \sim D^{-n}$ for micro- and nano-pillar compression[1,3], where σ is the yielding strength, D the pillar diameter and n the material specific exponent; $H = H_0\sqrt{1+\frac{h^*}{h}}$ for nanoindentation[3,8,9], where H is the hardness for a given indentation depth h, H_0 the size-independent hardness and h^* the material specific length scale that also depends on the shape of an indenter. In theory, these scaling relations all stem from dislocations, the "plasticity carrier" in crystalline materials whose nucleation and movement are essentially size dependent[10-12].

Interestingly, metallic glasses (MGs) exhibit a similar size effect[13-28] despite the lack of a long-range crystalline structure and crystalline-like defects, such as dislocations. Many research groups[13-28] found that the strengths of MGs could increase relative to the bulk values in nanoindentation or micro- and nano-compression. To rationalize this size effect, a number of theories were proposed, such as Weibull statistics[14,19,26] and size-dependent shear band nucleation[27,29,30]. The recent molecular dynamics (MD) simulations[31] even showed that, as the sample size reduces to the nanometer scale, the shear strength of a MG could rise up from the bulk value of about ~G/50 (G=shear modulus) to an intrinsic strength limit of ~G/10. However, the issue of strength size effect in MGs is not yet fully settled. There were other experimental results obtained from micro- and nano-compression[32-37], which showed no significant change in the strength of MGs with the decreasing sample size. A similar finding was also reported by Packard et al.[38] from the spherical nanoindentation of a few kinds of MGs. Interestingly, it could be observed from the work of Packard et al.[38] that the hardness of the MGs

slightly decreased rather than increased with the decreasing tip radius. This “inverse” size effect was then attributed to a possible surface effect[38].

To reconcile the seeming discrepancy among many previous findings, one possible explanation is that shear band nucleation in MGs is not only size dependent but also affected by a sample surface at the nanometer scale. Conceptually, this is analogous to homogeneous versus heterogeneous nucleation of shear bands as discussed recently in Refs.[23,30]. Taking into account the possible surface effect that usually facilitates shear band nucleation, one may envision that bulk nucleation of shear bands in MGs would be “interrupted” by surface controlled shear band nucleation when the size of a sample or deformation field approaches a critical value as depicted in Fig. 1. Around this critical size, the usual scaling relation for the strength of MGs would break down with no obvious trend of size effect. Meanwhile, significant data scattering might appear around this critical size as the strength of MGs becomes very sensitive to the shear band nucleation site. At the present time, however, there is no definitive answer to whether such a critical size exists and, if it does, what determines the critical size in different kinds of MGs.

To address the above issue, we chose six MGs, including $Zr_{52.5}Cu_{17.9}Ni_{14.6}Al_{10}Ti_5$, $La_{60}Al_{25}Ni_{15}$, $Au_{49}Ag_{5.5}Pd_{2.3}Cu_{26.9}Si_{16.3}$, $Pd_{40}Cu_{30}P_{20}Ni_{10}$, $Fe_{48}Cr_{15}Mo_{14}C_{15}B_6Er_2$ and $(Fe_{44.3}Cr_5Co_5Mo_{12.8}Mn_{11.2}C_{15.8}B_{5.9})_{98.5}Y_{1.5}$ (in at.%), to study the possible break-down of the strength size scaling with spherical indentation. These alloys cover a wide range of mechanical/physical properties and their glassy nature was already identified by X-ray diffraction (XRD) (see Refs[27,39,40]) and the sample surface was mechanically polished to a mirror finish. Their basic mechanical properties, including elastic modulus and

hardness, were first measured on the Hysitron™ NanoIndenter system (Hysitron Inc, Minneapolis, MN) with a Berkovich diamond tip (see Table 1). Subsequently, a series of spherical nanoindentation experiments were carried out at the constant indentation strain rate $\dot{\varepsilon} = 0.2s^{-1}$ with the indenters of nine different radii R (R=0.1, 0.4μm, 2μm, 5μm, 10μm, 20μm, 25μm, 30μm and 35μm). According to the Hertzian theory, we can extract the reduced modulus E_r by fitting the initial linear portion of the P-$h^{3/2}$ curve to $P = (4E_rR^{1/2}/3)h^{3/2}$, where P is the indentation load and h the indentation depth. The results agree well with the Berkovich nanoindentation results. Following Ref.[30], the critical yielding load P_c is herein identified to be the point of departure of the P-h curve from the Hertzian solution. Here, it is interesting to note that, for the Zr-based MG in our study, the departure from the Hertzian curve appears abrupt and almost coincides with the point of the first pronounced displacement pop-in for the small indenters (R≤2μm), which is consistent with the previous reports[38,41]; however, the point of departure turns into a gradual and smooth elasto-plastic transition for the large indenters (R>2μm). A similar phenomenon was also observed in other MGs, which suggests that local plasticity should have set in before the first pronounced displacement pop-in in the indentation of MGs, particularly so for the indentation with the large indenters. In the literature[26,30,42], a similar behavior of incipient plasticity disconnected with the first conspicuous pop-in event was also found in various experiments and/or atomistic simulations. Theoretically, this could be attributed to the formation of constrained shear bands or the activation[30,43] of shear transformation zones (STZs) in the early stage of incipient plasticity[30,31,38,44].

Once E_r and P_c are obtained, the hardness H or critical pressure p_c for yielding under the indenter can be obtained as $H = p_c = \left(\frac{6PE_r^2}{\pi^3 R^2}\right)^{\frac{1}{3}}$ for various indenter tip radius R and different MG compositions. As an estimation, the yield strength σ of the MGs is approximated as the measured hardness H divided by three[45,46]. Interestingly, regardless of the chemical composition, the yield strength σ exhibits a sharp and positive size effect when R is above a critical value while a negative size effect when below, as shown in Figs. 2(a)-(f). This critical indenter size is found to be ~2μm for the Zr-based MG but seen to vary with the chemical composition of the MGs studied [Figs. 2(a)-(f)].

To quantitatively understand the positive size effect, we first apply the scaling relation derived in our previous work[30] to fit the experimental data. By assuming that yielding is triggered by homogenous shear-band nucleation[23-25,47,48], it can be derived $H = H_0 + 0.54E_r(l_c/R)^{\frac{3}{2}}$, where H is the size dependent hardness, H_0 the "bulk" hardness and l_c the critical size for homogenous shear-band nucleation defined in Ref.[30]. Therefore, we obtain:

$$\sigma = \sigma_0 + 0.18E_r\left(\frac{l_c}{R}\right)^{\frac{3}{2}} \quad (1)$$

where $\sigma = H/3$ and $\sigma_0 = H_0/3$. As shown in Figs. 2(a)-(f), the above equation fits the experimental data very well in the regime of the positive size effect, from which l_c for various MGs was extracted and are listed in Table 1 . The critical size l_c characterizes the size for the transition of the constrained and slowly growing shear band to an unconstrained autocatalytically growing shear band. In general, it can be perceived that

the critical indenter tip radius increases with the critical length scale l_c. In other words, one may view that the break-down of the strength-size scaling is controlled internally by the length scale l_c and externally by the tip radius R.

Before we get into the physical origin of l_c, let us briefly discuss the possible mechanism for the "inverse" size effect seen in Figs. 2(a)-(f). As aforementioned, unlike the homogeneous shear band nucleation, yielding in MGs could be controlled by a surface mediated process. This idea is supported by the recent in-situ nanoindentation of MGs conducted under a transmission electron microscope (TEM)[49], which clearly showed that a subsurface local plastic zone formed at a low stress, gradually spread out from their initiation sites with the increasing stress, and finally joined the tip-surface contact to cause overall yielding. Conceptually, this is similar to the shear plane yielding criterion proposed by Packard *et al.*[38,50], who conjectured that yielding occurs in spherical indentation of MGs once a well-defined shear plane can be established between the shear-band initiation site and a sample surface. According to our theoretical model[30], however, this is possible only when the shear-band initiation site is very close to a sample surface. Since the distance from the sample surface to the shear band initiation site scales with the tip radius under spherical indentation, the surface mediated shear band initiation therefore becomes effective only when the tip radius is below a certain value. This is consistent with our findings as demonstrated in Figs. 2(a)-(f). At the present time, the inverse size effect can be qualitatively interpreted to be due to a weak surface, as suggested by Packard et al[38], which offers less resistance to shear band initiation than the bulk in our study.

Since our data suggest that all MGs possess a "soft" surface in resisting shear band initiation, the break-down of the strength size scaling is controlled mainly by l_c, the critical size for a constrained shear band to grow into an autocatalytic growing "defect". According to Refs[30,43,51] , we have $l_c = \frac{\alpha t_{SB}}{W} G$, where α~1.16 is a dimensionless factor; W is the shear softening rate within the constrained shear band (the strength loss per unit strain), which generally varies with the applies strain rate[30], the thermal history of a MG[43] and its chemical makeup; and t_{SB} is the shear-band thickness, which can be regarded as a constant (10-20 nm) according to Refs[52,53]. As shown in Fig. 3(a), the data of l_c versus G can be roughly fitted to a linear relation (the red line in Fig. 3(a)) despite the data scattering. The data spreading suggests that the slop of t_{SB}/W varies with the chemical composition of the MG. From the slop of the l_c versus G curve, we can extract the shear softening rate W for different MGs at a given shear band thickness (=10 nm). Interestingly, we find that the shear softening rate W is correlated very well with the Poisson's ratio ν of the individual MG, as listed in Table 1 and shown in Fig. 3(b). This correlation is intriguing and must be rationalized.

According to the prior works[54-59], MGs are intrinsically heterogeneous at the nanometer scale, containing soft regions dispersed in an elastic amorphous matrix. According to the recent work of Sun et al.[60], the Poisson's ratio can be taken as a metric of the elastic heterogeneity intrinsic to a MG, i.e., a higher Poisson's ratio corresponds to more significant elastic heterogeneities and *vice versa*. Therefore, if the subcritical growth of a constrained shear band involves the linkage of the soft regions, as recently revealed by the dynamic atomic force microscopy[61], the softening rate W should simply

measure how much local strength is lost in an amorphous when it is locally converted into a soft region for the extension of an embryonic shear band. Since the strength and modulus are correlated to each other for MGs[62], the softening rate W should be correlated with the elastic heterogeneity and thus the Poisson's ratio, as seen in Fig. 3(b).

Before moving to the summary, let us discuss the implications of the current work pertaining to micro- and nano-compression of MGs. Fig.4 displays the published micro- and nano-compression data of the Zr-based MGs[14,15,28,35,63], from which one may perceive a general size effect as the pillar strengths are always above the corresponding bulk value. Nevertheless, it is interesting to note that the yielding strengths of the Zr-based MG micropillars exhibit very strong scattering when the pillar size D was reduced to below 1 μm. Within that size regime (D < 1 μm), there is no obvious trend of strength size scaling. This behavior is consistent very well with the aforementioned size-controlled transition from bulk to surface mediated shear band initiation (Fig. 1). By assuming that yielding was controlled by shear band initiation within the pillar, Wang et al[34] derived a strength-size scaling relation $\sigma^2 - \sigma_0^2 = \frac{\psi}{D}$ for the micro- and nano-compression of MGs, where σ is the size-dependent strength ; σ_0 is the size-independent strength for the bulk material; D is the top diameter of the pillar and ψ is the parameter that depends on the modulus, sample aspect ratio and energy consumption per unit area of shear banding. Rearranging the above equation leads to $\sigma = \sigma_0\sqrt{1+\frac{l_c^*}{D}}$, where l_c^* is the critical length scale $=\psi/\sigma_0$, which plays a similar role as l_c in Eq. 1. Similar to Figs. 2(a)-(f), we can fit the above scaling relation to the micro- and nano-compression data that follow a positive size effect (the envelope of the data in Fig. 4). Interestingly, the l_c^* extracted from the data fitting

falls into a narrow range between 0.4 and 0.8μm, which compares very well with l_c = 0.54 μm we extracted from the nanoindentation of the Zr-based MG.

To summarize, we demonstrate the break-down of the strength size scaling in MGs with spherical indentation in this work. Physically, this is attributed to the transition of the yielding mechanism from bulk or homogeneous shear band nucleation to surface mediated shear band nucleation. The critical size that controls the transition is found to correlate with the shear modulus and Poisson's ratio of a MG. Furthermore, the significant data scattering of the yield strengths obtained from micro- and nano-compression of MGs can be rationalized within the current theoretical framework.

Acknowledgements

The research of YY is supported by the research grant council (RGC), the Hong Kong government, through the general research fund (GRF) with the grant number of 11207215.

Reference

[1] J. R. Greer and J. T. M. De Hosson, Prog Mater Sci **56** (6), 654 (2011).

[2] Y. T. Cheng and C. M. Cheng, Mat Sci Eng R **44** (4-5), 91 (2004).

[3] W. D. Nix and H. J. Gao, J Mech Phys Solids **46** (3), 411 (1998).

[4] G. M. Pharr, E. G. Herbert, and Y. F. Gao, Annual Review of Materials Research, Vol 40 **40**, 271 (2010).

[5] M. R. Begley and J. W. Hutchinson, J Mech Phys Solids **46** (10), 2049 (1998).

[6] J. G. Swadener, E. P. George, and G. M. Pharr, J Mech Phys Solids **50** (4), 681 (2002).

[7] A. G. Evans and J. W. Hutchinson, Acta Mater **57** (5), 1675 (2009).

[8] Yanfei Gao and Hongbin Bei, Prog Mater Sci **82**, 118 (2016).

[9] W. C. Oliver and G. M. Pharr, J Mater Res **7** (6), 1564 (1992).

[10] Julia R. Greer, Warren C. Oliver, and William D. Nix, Acta Mater **53** (6), 1821 (2005).

[11] M. D. Uchic, D. M. Dimiduk, J. N. Florando, and W. D. Nix, Science **305** (5686), 986 (2004).

[12] D. M. Dimiduk, M. D. Uchic, and T. A. Parthasarathy, Acta Mater **53** (15), 4065 (2005).

[13] C. J. Lee, J. C. Huang, and T. G. Nieh, Appl Phys Lett **91** (16) (2007).

[14] Y.H. AU - Lee Lai, C.J. AU - Cheng, Y.T. AU - Chou, H.S. AU - Chen, H.M. AU - Du, X.H. AU - Chang, C.I. AU - Huang, J.C. AU - Jian, S.R. AU - Jang, Scripta Mater **58** (10) (2008).

[15] D. C. Jang and J. R. Greer, Nature Materials **9** (3), 215 (2010).

[16] D. C. Jang, C. T. Gross, and J. R. Greer, Int J Plasticity **27** (6), 858 (2011).

[17] I. C. Choi, Y. Zhao, Y. J. Kim, B. G. Yoo, J. Y. Suh, U. Ramamurty, and J. I. Jang, Acta Mater **60** (19), 6862 (2012).

[18] J. I. Jang, B. G. Yoo, Y. J. Kim, J. H. Oh, I. C. Choi, and H. B. Bei, Scripta Mater **64** (8), 753 (2011).

[19] C. J. Lee, Y. H. Lai, J. C. Huang, X. H. Du, L. Wang, and T. G. Nieh, Scripta Mater **63** (1), 105 (2010).

[20] L. Tian, Y. Q. Cheng, Z. W. Shan, J. Li, C. C. Wang, X. D. Han, J. Sun, and E. Ma, Nat Commun **3**, 619 (2012).

[21] C. C. Wang, J. Ding, Y. Q. Cheng, J. C. Wan, L. Tian, J. Sun, Z. W. Shan, J. Li, and E. Ma, Acta Mater **60** (13-14), 5370 (2012).

[22] F. F. Wu, W. Zheng, S. D. Wu, Z. F. Zhang, and J. Shen, Int J Plasticity **27** (4), 560 (2011).

[23] A. L. Greer, Y. Q. Cheng, and E. Ma, Mat Sci Eng R **74** (4), 71 (2013).

[24] C. A. Schuh, T. C. Hufnagel, and U. Ramamurty, Acta Mater **55** (12), 4067 (2007).

[25] Y. Yang and C. T. Liu, J Mater Sci **47** (1), 55 (2012).

[26] J. C. Ye, J. Lu, Y. Yang, and P. K. Liaw, Intermetallics **18** (3), 385 (2010).

[27] Y. M. Lu, B. A. Sun, L. Z. Zhao, W. H. Wang, M. X. Pan, C. T. Liu, and Y. Yang, Sci Rep-Uk **6**, 28523 (2016).

[28] Ashwini Bharathula, Seok-Woo Lee, Wendelin J. Wright, and Katharine M. Flores, Acta Mater **58** (17), 5789 (2010).

[29] B. Yang, C. T. Liu, and T. G. Nieh, Appl Phys Lett **88** (22) (2006).

[30] S. Wang, Y. F. Ye, B. A. Sun, C. T. Liu, S. Q. Shi, and Y. Yang, J Mech Phys Solids **77**, 70 (2015).

[31] Y. Q. Cheng and E. Ma, Acta Mater **59** (4), 1800 (2011).

[32] B. E. Schuster, Q. Wei, T. C. Hufnagel, and K. T. Ramesh, Acta Mater **56** (18), 5091 (2008).

[33] B. E. Schuster, Q. Wei, M. H. Ervin, S. O. Hruszkewycz, M. K. Miller, T. C. Hufnagel, and K. T. Ramesh, Scripta Mater **57** (6), 517 (2007).

[34] C. A. Volkert, A. Donohue, and F. Spaepen, J Appl Phys **103** (8), 3539 (2008).

[35] A. Dubach, R. Raghavan, J. F. Loffler, J. Michler, and U. Ramamurty, Scripta Mater **60** (7), 567 (2009).

[36] C. Q. Chen, Y. T. Pei, and J. T. M. De Hosson, Acta Mater **58** (1), 189 (2010).

[37] J. T. M. De Hosson, Microsc Res Techniq **72** (3), 250 (2009).

[38] C. E. Packard and C. A. Schuh, Acta Mater **55** (16), 5348 (2007).

[39] Z. P. Lu, C. T. Liu, J. R. Thompson, and W. D. Porter, Phys Rev Lett **92** (24) (2004).

[40] S. X. Song, J. S. C. Jang, J. C. Huang, and T. G. Nieh, Intermetallics **18** (4), 702 (2010).

[41] H. Bei, Z. P. Lu, S. Shim, G. Chen, and E. P. George, Metall Mater Trans A **41A** (7), 1735 (2010).

[42] Y. H. Liu, C. T. Liu, W. H. Wang, A. Inoue, T. Sakurai, and M. W. Chen, Phys Rev Lett **103** (6) (2009).

[43] S. Wang, Y. F. Ye, S. Q. Shi, and Y. Yang, J Appl Phys **119** (24), 245113 (2016).

[44] J. Ding, Y. Q. Cheng, and E. Ma, Appl Phys Lett **104** (1) (2014).

[45] J. C. Ye, J. P. Chu, Y. C. Chen, Q. Wang, and Y. Yang, J Appl Phys **112** (5) (2012).

[46] H. S. Chen, J Appl Phys **49** (1), 462 (1978).

[47] A. Dubach, F. H. Dalla Torre, and J. F. Loffler, Acta Mater **57** (3), 881 (2009).

[48] F. Shimizu, S. Ogata, and J. Li, Acta Mater **54** (16), 4293 (2006).

[49] L. Gu, L. M. Xu, Q. S. Zhang, D. Pan, N. Chen, D. V. Louzguine-Luzgin, K. F. Yao, W. H. Wang, and Y. Ikuhara, Sci Rep-Uk **5**, 9122 (2015).

[50] C. E. Packard, E. R. Homer, N. Al-Aqeeli, and C. A. Schuh, Philosophical Magazine **90** (10), 1373 (2010).

[51] K. Uenishi and J. R. Rice, J Geophys Res-Sol Ea **108** (B1) (2003).

[52] M. Q. Jiang, W. H. Wang, and L. H. Dai, Scripta Mater **60** (11), 1004 (2009).

[53] Y. Zhang and A. L. Greer, Appl Phys Lett **89** (7) (2006).

[54] F. Leonforte, R. Boissière, A. Tanguy, J. P. Wittmer, and J. L. Barrat, Phys Rev B **72** (22), 224206 (2005).

[55] Y. Q. Cheng and E. Ma, Phys Rev B **80** (6), 064104 (2009).

[56] Y. Yang, J. F. Zeng, A. Volland, J. J. Blandin, S. Gravier, and C. T. Liu, Acta Mater **60** (13-14), 5260 (2012).

[57] J. C. Ye, J. Lu, C. T. Liu, Q. Wang, and Y. Yang, Nature Materials **9** (8), 619 (2010).

[58] Y. H. Liu, D. Wang, K. Nakajima, W. Zhang, A. Hirata, T. Nishi, A. Inoue, and M. W. Chen, Phys Rev Lett **106** (12), 125504 (2011).

[59] Y. Q. Cheng, A. J. Cao, and E. Ma, Acta Mater **57** (11), 3253 (2009).

[60] B. A. Sun, Y. C. Hu, D. P. Wang, Z. G. Zhu, P. Wen, W. H. Wang, C. T. Liu, and Y. Yang, Acta Mater **121**, 266 (2016).

[61] Y. M. Lu, J. F. Zeng, S. Wang, B. A. Sun, Q. Wang, J. Lu, S. Gravier, J. J. Bladin, W. H. Wang, M. X. Pan, C. T. Liu, and Y. Yang, Sci Rep-Uk **6**, 29357 (2016).

[62] W. H. Wang, Prog Mater Sci **57** (3), 487 (2012).

[63] Dongchan Jang, Cameron T. Gross, and Julia R. Greer, Int J Plasticity **27** (6), 858 (2011).

[64] Z. Bian, R. J. Wang, M. X. Pan, D. Q. Zhao, and W. H. Wang, Adv Mater **15** (7-8), 616 (2003).

[65] C. G. Tang, Y. Li, and K. Y. Zeng, Mat Sci Eng a-Struct **384** (1-2), 215 (2004).

[66] S. T. Liu, Z. Wang, H. L. Peng, H. B. Yu, and W. H. Wang, Scripta Mater **67** (1), 9 (2012).

[67] W. H. Wang, C. Dong, and C. H. Shek, Mat Sci Eng R **44** (2-3), 45 (2004).

[68] J. Schroers, B. Lohwongwatana, W. L. Johnson, and A. Peker, Appl Phys Lett **87** (6) (2005).

[69] U. Harms, O. Jin, and R. B. Schwarz, J Non-Cryst Solids **317** (1-2), 200 (2003).

[70] V. Ponnambalam, S. J. Poon, and G. J. Shiflet, J Mater Res **19** (5), 1320 (2004).

List of Figure Captions

Figure 1. The schematic illustration of the breakdown of strength-size scaling in metallic glass.

Figure 2. The size dependence of the normalized hardness for (a) $Zr_{52.5}Cu_{17.9}Ni_{14.6}Al_{10}Ti_5$, (b) $La_{60}Al_{25}Ni_{15}$, (c) $Au_{49}Ag_{5.5}Pd_{2.3}Cu_{26.9}Si_{16.3}$, (d) $Pd_{40}Cu_{30}P_{20}Ni_{10}$, (e) $Fe_{48}Cr_{15}Mo_{14}C_{15}B_6Er_2$ and (f) $(Fe_{44.3}Cr_5Co_5Mo_{12.8}Mn_{11.2}C_{15.8}B_{5.9})_{98.5}Y_{1.5}$.

Figure 3. The correlation between (a) the critical size l_c and shear modulus G, (b) Poisson's ratio v and shear softening rate W for various MGs.

Figure 4. The size dependence of the strength extract from previous micro-compression test results for Zr-based MG. Note that the various color solid lines show the estimation of the critical size for the shear band initiation according to the positive size effect.

List of Table Captions

Table 1. The reduced modulus (E_r), bulk hardness (H_0), size independent strength (σ_0) and the critical length scale (l_c) extracted from spherical nanoindentation for various MGs; the yielding strength (σ_y) and the Poisson's ratio (v) for various MGs from literature.

List of Figures

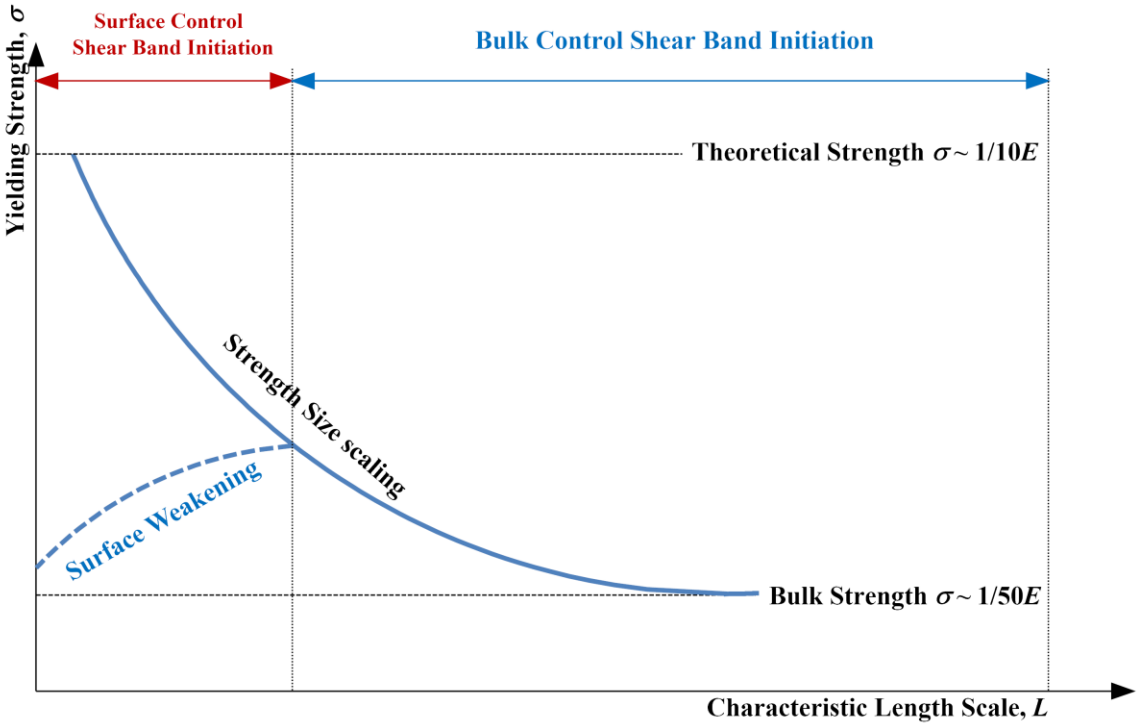

Figure 1. Wang et al.

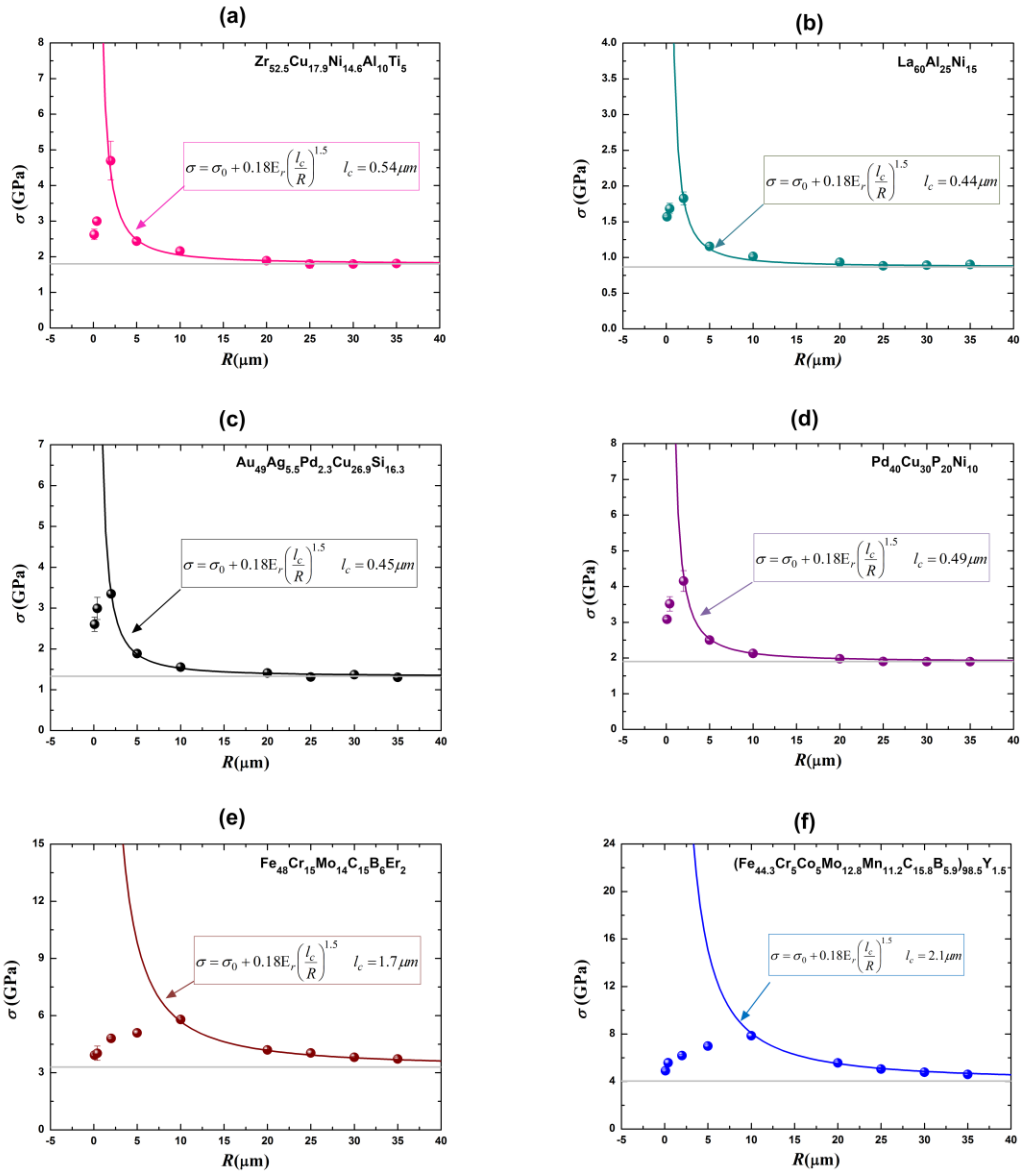

Figure 2. Wang et al.

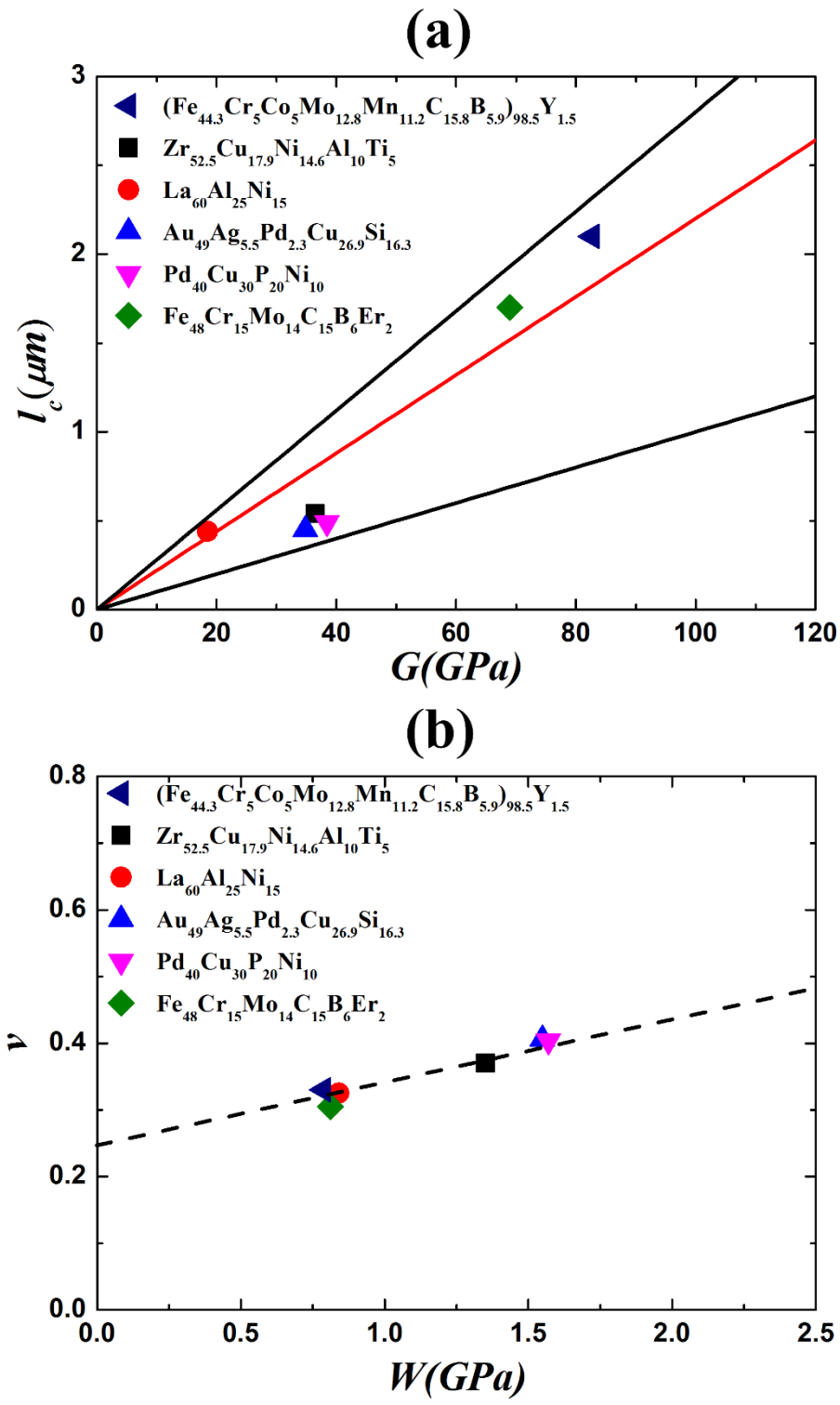

Figure 3. Wang et al.

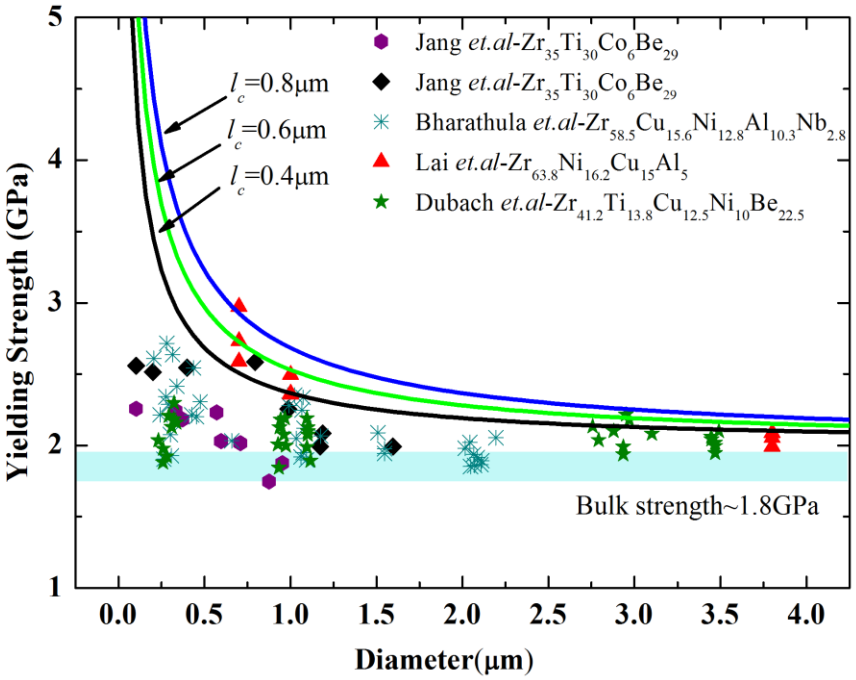

Figure 4. Wang et al.

List of Tables

Table 1. Wang et al.

Composition	E_r (GPa)	H_0 (GPa)	σ_0	l_c (μm)	ν	σ_y
$Zr_{52.5}Cu_{17.9}Ni_{14.6}Al_{10}Ti_5$	100±2	5.4±0.3	1.8	0.54	0.370[64]	1.8[65]
$La_{60}Al_{25}Ni_{15}$	49±2	2.7±0.2	0.9	0.44	0.325[66]	0.9[67]
$Au_{49}Ag_{5.5}Pd_{2.3}Cu_{26.9}Si_{16.3}$	97±2	4.0±0.3	1.3	0.45	0.406[68]	1.2[68]
$Pd_{40}Cu_{30}P_{20}Ni_{10}$	107±3	5.7±0.3	1.9	0.49	0.404[62]	1.8[69]
$Fe_{48}Cr_{15}Mo_{14}C_{15}B_6Er_2$	177±5	9.9±1.3	3.3	1.7	0.305[62]	3.2[70]
$(Fe_{44.3}Cr_5Co_5Mo_{12.8}Mn_{11.2}C_{15.8}B_{5.9})_{98.5}Y_{1.5}$	222±9	12.1±1.5	4.0	2.1	0.33[26]	4.9[39]